“BABEŞ-BOLYAI” UNIVERSITY CLUJ-NAPOCA

FACULTY OF PHYSICS

MASTER IN BIOPHYSICS AND MEDICAL PHYSICS

MASTER THESIS

TRAUMATIC BRAIN INJURY RAPID DIAGNOSIS USING GOLD NANOPARTICLES AND ANTI GLIAL FIBRILARY ACIDIC PROTEIN BIOCONJUGATES IN A LATERAL FLOW IMMUNOASSAY

Scientific coordinator

Prof. Dr. Nicolae Leopold

Scientific co-coordinator

Prof. Dr. José Ricardo Ramos Franco Tavares

Faculdade de Ciências e Tecnologia, Universidade NOVA de Lisboa

Graduate

Oana-Maria Biro

2024

Aknowledgements

First of all, I would like to express my gratitude to my advisor, Professor Nicolae Leopold, for seeing the potential I have and driving me forward throughout the years, for the patience and perseverence, for all the support and insightful discussions. *Mulțumesc!*

To my co-advisor, Professor Ricardo Franco, for the opportunity to join his laboratory for five months, for all the helpful discussions and for showing me how to thoroughly analyse my work and strive for better! *Obrigada!*

To my wonderful Bionano team, to Cristina Freitas and Nuno Ferreira for all the knowledge they passed on to me, having patience with a physicist who had no idea what a BCA was. To the entire team, Hugo Marques and Raquel Carvalho for celebrating together the good results and working to figure out what went wrong with the bad ones, for the lunches, the DLS talks, the Wordles, for letting me share my culture with you and teaching me yours. To Simão Caracho for the insightful comments and for being the first one to give me a task in the lab. *Obrigada e até breve!*

To Professors Hugo Aguas, Henrique Vazão de Almeida, Rui Igreja, for showing me how a multidisciplinary team should be and for all the interesting meetings and discussions.

To my parents, for having patience with me and supporting me in discovering who I am and what I want to do, for always being there for me and for all the sacrifices they have made so I could explore the world. *Mulțumesc!*

CONTENTS

AKNOWLEDGEMENTS **3**

INTRODUCTION **7**

1. THEORY **9**

1.1. TRAUMATIC BRAIN INJURIES: DIAGNOSIS AND BIOMARKERS 9
1.2. LATERAL FLOW IMMUNOASSAYS 10
1.3. GOLD NANOPARTICLES IMMUNOTAGS 13

2. MATERIALS AND METHODS **15**

2.1. GOLD NANOPARTICLES SYNTHESIS AND CHARACTERIZATION 15
2.1.1. SPHERICAL GOLD NANOPARTICLE SYNTHESIS 15
2.1.2. AUNPS UV-VIS SPECTROSCOPY CHARACTERISATION 15
2.1.3. AUNPS FUNCTIONALISATION 16
2.1.4. DYNAMIC LIGHT SCATTERING (DLS) MEASUREMENTS 17
2.1.5. AUNPS COLLOIDAL STABILITY 17
2.2. DEVELOPMENT AND CHARACTERIZATION OF BIOCONJUGATES WITH HUMAN SERUM ALBUMIN (HSA) 18
2.2.1. BICINCHONINC ACID ASSAY FOR TOTAL PROTEIN DETERMINATION 18
2.2.2. CONJUGATION THROUGH PHYSISORPTION 19
2.2.3. AGAROSE GEL ELECTROPHORESIS (AGE) 19
2.3. DEVELOPMENT AND CHARACTERIZATION OF BIOCONJUGATES WITH ANTI - HORSERADISH PEROXIDASE (AHRP) 20
2.3.1.CONJUGATION THROUGH PHYSISORPTION 20
2.3.2.CONJUGATION THROUGH COVALENT LINKING 20
2.3.3.HRP ENZYMATIC ACTIVITY ASSAY 21
2.4. LATERAL FLOW ASSAY FABRICATION 21
2.4.1. LATERAL FLOW DISPENSER 21
2.4.2. MEMBRANE SELECTION 22

3. RESULTS AND DISCUSSION 23

3.1. GOLD NANOPARTICLES 23
3.1.1. SYNTHESIS AND CHARACTERIZATION 23
3.1.2. MODIFICATION WITH 11-MUA 25
3.1.3. COLLOID STABILITY 26
3.2. BIOCONJUGATES WITH HSA 28
3.2.1. BICINCHONINIC ACID ASSAY FOR TOTAL PROTEIN DETERMINATION 28
3.2.2. CONJUGATION THROUGH PHYSISORPTION 29
3.3. BIOCONJUGATES WITH AHRP 31
3.3.1. CONJUGATION THROUGH PHYSISORPTION 31
3.3.2.*CONJUGATION THROUGH COVALENT LINKING 33
3.4. LATERAL FLOW ASSAY FABRICATION 35
3.4.1. LATERAL FLOW DISPENSER 35
3.4.2. MEMBRANE SELECTION 36

CONCLUSIONS AND FUTURE PERSPECTIVES 39

REFERENCES 41

Introduction

Traumatic brain injuries (TBI) are a significant global health concern, with an annual incidence of 69 million cases. [1] The causes for TBI are diverse, ranging from household accidents such as falls or head bumps, to more severe incidences such as traffic accidents, assaults, and sports injuries – particulary in contact sports such as martial arts, boxing or rugby. While the majority of these injuries (approximately 81%) are classified as mild (mTBI) [1], they still result in physical, cognitive and emotional symptoms, sending the patients to the emergency room and putting a burden on the healthcare system. Under the current protocols, patients typically spend several hours in the emergency department, undergo a physical assessment using tools such as the Glasgow Coma Scale and recieve a CT scan (which often fails to detect abnormalities in mTBI cases) begore being discharged without a follow-up plan or a clear understanding of potential symptoms. Consequently, half of mTBI patients experience neurocognitive problems in the first month after the accident, some of them manifesting sequelae at one year afterwards. [2]

The emerging paradigm for diagnosing mTBI involves the use of bloodborne biomarkers which are brain-specific and can indicate both the presence of an injury and its severity. Several studies indicate the possible use of glial fibrillary acidic protein (GFAP) in the detection of traumatic brain injuries [3], [4], [5], [6]. GFAP is an intermediate filament III protein integral to the cytoskeletal structure of glial cells, providing mechanical strength. In response to brain injuries, astroglial cells undergo hypertrophy, resulting in increased GFAP expression and proliferation. [7] Post-trauma, GFAP and its breakdown products are released into the interstitial fluid and subsequently enter the bloodstream. Therefore, by analyzing a blood sample, the levels of GFAP can be measured to assess the presence of injury, as well as its severity by creating a calibration curve.

Lateral flow immunoassays are widely used diagnostic tests (e.g. pregnancy tests, COVID-19 rapid antigen tests) that offer the potential for rapid, cost-effective, point-of-care testing. These colorimetric assays often utilize gold nanoparticles due to their intense red color and their ability to form bioconjugates with antibodies, which act as detection mechanisms by capturing the target protein and accumulating on the test line.

The aim of this research is to develop a lateral flow immunoassay for the detection of traumatic brain injuries, using gold nanoparticle bioconjugates with specific antibodies. Given the high costs associated with GFAP antibodies and protein, an initial test system using horseradish peroxidase (HRP) as a model complex is employed for optimization. This involves synthesizing and functionalizing gold nanoparticles, and testing them in sandwich assays to optimize the test system.

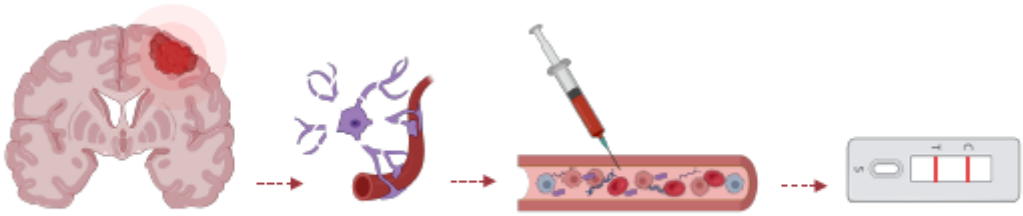

Figure 1. Glial fibrillary acidic protein is a major constituent of the astroglial cytoskeleton that gets released into the blood stream in case of astrocyte damage. The brain specific biomarker can then be used in a lateral flow assay for the detection of traumatic brain injuries**.**

This thesis is structured into four chapters: a theoretical chapter explaining the background of the research, a materials and methods chapter detailing the experimental setup and methodology, a results and discussion chapter presenting and analyzing the findings, and a conclusion and future perspectives chapter.

Furthermore, the work presented in this thesis was showcased as a poster presentation at the 13th International Conference on Clinical Spectroscopy (SPEC 2024) held in Ioannina, Greece, from June 2-6, 2024.

1. Theory

1.1. Traumatic brain injuries: diagnosis and biomarkers

Traumatic brain injuries (TBI) are among the most prevalent neurological issues, significantly impacting global health. They represent the leading cause of death and disability among trauma-related injuries worldwide, having a critical role in both mortality and long-term impairment. [1] The injuries are caused by external forces, which damage the brain tissue and lead to primary and secondary injuries. While the primary injury occurs immediately after impact, the secondary injury consists of brain swelling and biochemical changes in the brain, which in turn lead to hypoxia and cell death. [8] This secondary injury is the most damaging one, increasing the likelihood of a poor patient outcome. Early identification of traumatic brain injuries can lower the risk of sequelae and improve patient outcome. [9]

Currently, TBIs are diagnosed through neurological assessments such as the Glasgow Coma Scale, whose rating evaluates the injuries in three categories: mild (mTBI), moderate or severe. The Glasgow Coma Scale looks at the level of consciousness, verbal, motor and eye-opening responses to stimuli, but is limited in detecting the subtle cognitive impairments associated with mTBI.

Other current methods of diagnosis include imaging techniques such as Computed Tomography (CT) scans or Magnetic Resonance Imaging (MRI). The first one is the most common practice for patients in emergency settings, as it can rule out life-threatening conditions such as hemmorages. Nonetheless, CT scans often miss to identify mTBIs as these do not show visible structural changes. Moreover, CT scans use ionizing radiation, posing a health concern for the patients. MRIs on the other hand, are harmless to the patient and offer a more detailed view of the brain. However, besides being unavailable in many places, they are both time and money consuming and consist of an additional burden to the healthcare system.

The newest paradigm in diagnosing traumatic brain injuries is by using blood borne biomarkers which can indicate the presence of brain tissue damage. Biomarkers could be proteins, genes, or specific molecules which indicate a biological process pertaining

to a medical condition. Brain specific biomarkers have been recently studied in order to find new ways of diagnosing and monitoring neurological diseases such as traumatic brain injuries or strokes.

s100 calcium binding protein beta (s100B) has been studied, elevated concentrations indicating secondary injury progression and a possible poor outcome [10]. Another marker associated with severe TBI could be inflammatory cytokines, such as Interleukin (IL) - 1β, -6, -8, -10 [11]. In spite of studies linking these markers to TBIs, they are not brain specific and could indicate an inflammation somewhere else in the body.

Glial fibrillary acidic protein (GFAP) is a brain specific protein, with a long enough half-life suited for analysis. [12] The fast increase in blood GFAP concentration post-injury is another advantage for using it as a biomarker for the fast diagnosis of TBIs. [13] GFAP is the principal intermediate filament that maintains the mechanical strength of astrocytes and supports neighbouring neurons, as well as the blood-brain barrier. [7] When a brain injury occurs, astroglial cells undergo cellular hypertrophy and proliferation, which in turn elevates the GFAP content. [14] The release of high amounts of GFAP from injured astrocytes into the interstitial fluid, leads to its infiltration through the blood-brain barrier into the blood stream. Studies show that GFAP levels are elevated within 3 to 34h in serum/pasma post-injury. [15]

As such, a blood sample could potentially be used to detect the elevated levels of GFAP and diagnose TBIs in emergency settings, leading to quick treatment which will improve the outcome of the patient and reduce the secondary injuries.

1.2. Lateral flow immunoassays

Liquid chromatography (LC), mass spectrometry (MS), enzyme-linked immunosorbent assay (ELISA), and lateral flow assays (LFAs) are essential techniques for detecting and quantifying proteins such as glial fibrillary acidic protein (GFAP) in biological samples. LC, particularly when coupled with MS (LC-MS/MS), provides high sensitivity and specificity, enabling precise quantification of GFAP in human plasma. [16] ELISA is

another widely used technique, offering high sensitivity and specificity for protein detection. Studies have validated an ELISA for GFAP, showcasing its potential as a diagnostic tool for traumatic brain injury. [17] Despite the high accuracy and detailed analysis offered by LC, MS, and ELISA, they require specialized equipment and expertise, making them less suitable for point-of-care settings.

In contrast, LFAs provide a rapid, cost-effective, and user-friendly alternative, delivering results within minutes without the need for specialized equipment or extensive training. This makes LFAs the optimal choice for fast and reliable point-of-care testing, particularly in resource-limited environments. [18] They are also very simple to use: the sample is added onto the strip and after a short incubation time, a colored line appears indicating the test outcome as positive or negative. [19]

LFAs are based on two systems: the movement of sample via capillary force and an immunochemical reaction between the target and its capture molecule. It contains a sample pad, on which the sample matrix (blood, urine, plasma, etc.) is deposited, a conjugate pad, which contains tags coated in biorecognition elements, a nitrocellulose membrane on which the test and control line capture bioreceptors are deposited and an absorbent pad which drives the sample through the membrane, as shown in Figure 1.

Competitive and sandwich immunoassays are two fundamental formats used in LFAs, each offering distinct advantages and applications. In a competitive LFA, the target analyte competes with a labeled analyte for binding to a limited number of capture antibodies immobilized on the test line. The amount of labeled analyte that binds inversely correlates with the concentration of the target analyte in the sample, making it suitable for detecting small molecules like hormones or toxins. In contrast, sandwich LFAs use two distinct antibodies: one immobilized on the test line as a capture antibody and another labeled antibody that acts as an immunotag of the target analyte, forming a "sandwich" complex. This format allows for greater sensitivity as both antibodies must bind the analyte simultaneously, making it ideal for larger molecules such as proteins or viruses. In the case of GFAP detection, a sandwich immunoassay is the best option, as the target analyte is a protein. [18]

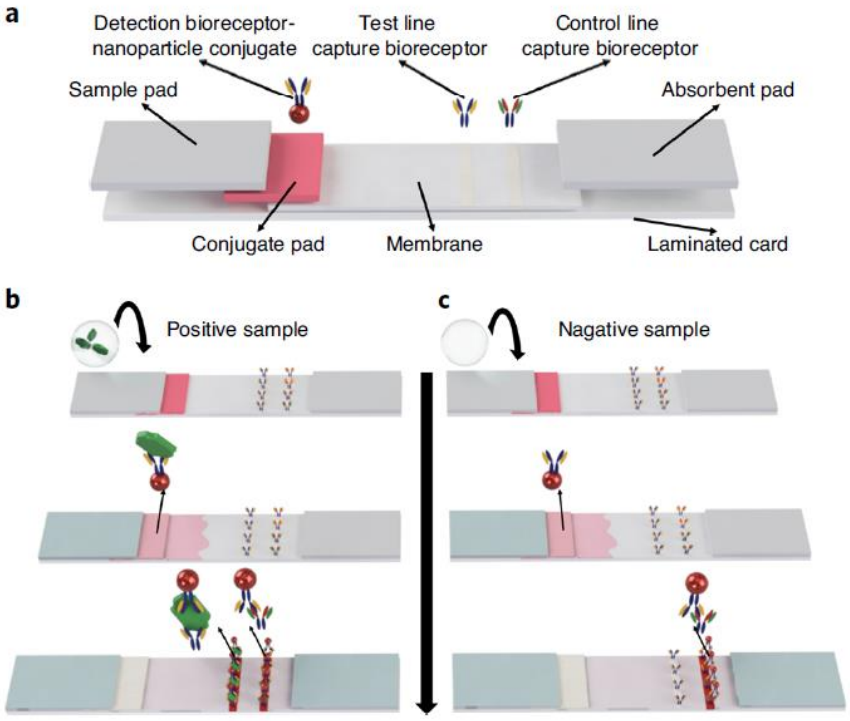

Figure 1.1 a. The main components of an LFA; b, c. The working principles in case of a positive or negative sample: the presence of the target analyte leads to the immunotags accumulating on the test and control lines, leading to a positive result (*Figure taken from* [19])

Figure 1.1 takes a closer look at the working principle of a sandwich immunoassay. The sample is applied on the sample pad, which ensures that its characteristics (viscosity, ionic strength, pH, etc) are optimal for the detection of the target analyte. Next, the sample flows to the conjugate pad which contains the labeled detection bioreceptors (in this case bioconjugates of gold nanoparticles and anti-GFAP antibodies). These bioconjugates are released when the sample wets the pad, leading to the interaction between the analytes in the sample and the bioconjugates. The solution then flows through the nitrocellulose membrane, where two lines are featured: the test line, which contains capture bioreceptors for the target analyte; and the control line, which contains capture bioreceptors for the bioconjugates. In case of a positive result, the bioconjugates and target analyte accumulate on the test line, which can be observed by the naked eye or via an optical reader. The role of the control line is to ensure the LFA is working correctly, and the sample reaches the end of the membrane. The final element is an absorbent pad, providing sufficient volume for complete sample flow. [19]

1.3. Gold nanoparticles immunotags

The most common labels used for LFAs are gold, silver, carbon nanoparticles, latex beads, quantum dots. [20] Gold nanoparticles are the most widely used labels due to their many advantages:

- There are multiple synthesis methods allowing for the fabrication of AuNPs in many different shapes and sizes;
- Their surface plasmon resonance (SPR) yields a vivid colour dependant on their shape and size, making them highly tunable to specific needs (for example, AuNPs < 30 nm have a very intense red colour);
- They have low toxicity, making them ideal for using with biological samples;
- They offer considerable stability in different conditions;
- They can be easily modified and functionalized through either physisorption or covalent binding, to create specific bioconjugates. [19]

As the shape, size and colour are important parameters that influence the successful fabrication of an LFA, the synthesis characteristics have to be chosen carefully. Small nanoparticles yield less intense colour, but are more stable, while large nanoparticles aggregate easily. [18] Another important factor to be considered is the ability of the nanoparticles to bind the capture molecule (e.g. anti-GFAP). Furthermore, the stability of the bioconjugates has to be taken into account as well as the blocking of any non-specific binding.

One of the most common methods to synthesize gold nanoparticles is a “bottom-up” approach developed by Turkevich [21] which implies the reduction of a metal salt ($HAuCl_4$) by using trisodium citrate both a reducing agent and as a capping agent. An improvement to this method was brought by Ojea-Jimenez [22] who changed the order of the reagent additions, which in turn resulted in an improvement in the shape and size distribution.

In order to fabricate capture immunotags, gold nanoparticles need to be functionalized with a bioreceptor. The first step would be to modify the nanoparticles by coating them in

a stabilizing molecule, such as mercaptobenzoic acid (MBA) or mercaptoundecanoic acid (MUA) which both have thiol groups that anchor them to the nanoparticles as well as carboxylic groups that act as a linker to biomolecules. As such, they play a double role: that of stabilizing agent, increasing the stability of the colloidal nanoparticles, as well as a linker between the AuNPs and the antibodies.

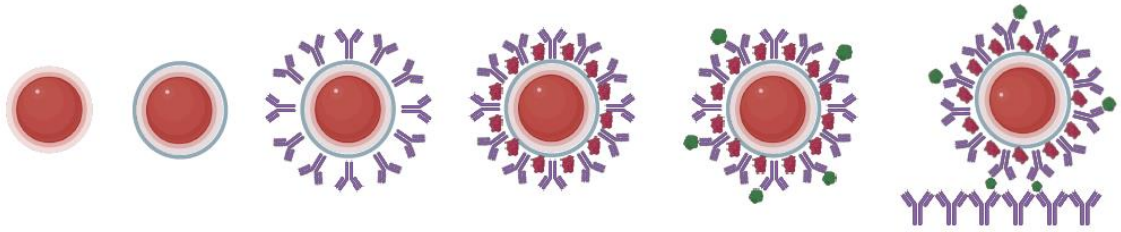

Figure 1.2 Schematic representation of the gold nanoparticles – antibodies immunotags in a sandwich assay; from left to right: AuNP, AuNP-MUA, AuNP-MUA-aHRP, AuNP-MUA-aHRP-BSA, AuNP-MUA-aHRP-BSA-HRP, AuNP-MUA-aHRP-BSA-HRP-aHRP

The second step is to conjugate the nanoparticles with the target antibody, which can be done either through physisorption or covalent linking. Another necessary step is to use another protein such as bovine serum albumin (BSA) as a blocking agent, which binds to the empty spaces on the nanoparticles left after the conjugation with antibodies. This is necessary to inhibit the non-specific binding of the bioconjugates.

2. Materials and methods

2.1. Gold nanoparticles synthesis and characterization

2.1.1. Spherical gold nanoparticle synthesis

The method used for synthesis was a modified version of the conventional synthesis process developed by Turkevich [21], advanced by Ojea-Jimenez [22] which improves the monodispersity and uniform spherical shape of the gold nanoparticles. All glassware and magnetic stirrers were washed beforehand with aqua regia (a 1:3 mixture of nitric acid and hydrochloric acid) to disolve any inert metals which could have been present on the surface and could potentially induce contamination or aggregation [23].

A volume of 98 ml of ultrapure water was added to an Erlenmeyer flask and placed on a heating element under reflux to assure constant reaction volume and concentration. The volume was stirred at 700 rpm using a magnetic stirrer. A volume of 2 ml trisodium citrate was added to the flask which was covered in aluminum foil to keep away from sunlight. After bringing the solution to boiling, 69.2 µl of a 1.445 M $HAuCl_4$ solution were added to induce the gold reduction reaction. After the passing of 5 minutes, the heating and stirring were stopped, terminating the reaction. The flask was then cooled to room temperature. Afterwards, the AuNPs solution was characterised and subsequently stored at 4°C, in an aluminum covered container to keep away from sunlight exposure.

2.1.2. AuNPs UV-Vis spectroscopy characterisation

The gold nanoparticles were characterised through UV-Vis spectroscopy (UV-Vis spectrophotometer Cary 50 Bio, Varian, San Francisco, USA), using 1 cm light pathway quartz cells in the range of 350 to 800 nm.

The formula devised by Haiss [24] which correlates the AuNPs diameter with their extinction coefficient ($\varepsilon_{450\,nm}$) allowed us to calculate the size and concentration of the previously synthesized nanoparticles.

By using the ratio between the absorbance of the localized surface plasmon resonance (A_{LSPR}) and the absorbance at 450 nm (A_{450}), it is possible to determine the diameter of the nanoparticles if it is in the range of 5-100 nm:

$$diameter(y) = 0.112e^{2.998\times\left(\frac{A_{LSPR}}{A_{450}}=x\right)} \quad (2.1)$$

The extinction molar coefficient can be determined as a function of the natural logarithm of the average AuNPs diameter:

$$ln\varepsilon_{450}(y) = 3.0869 \times \ln diameter(x) + 10.869 \quad (2.2)$$

By using the Beer-Lambert law [25], we can calculate the final concentration of the AuNPs solution:

$$C = \frac{A_{450\,nm} \times 1 \times Dilution\ Factor}{\varepsilon_{450\,nm}} \quad (2.3)$$

2.1.3. AuNPs functionalisation

The synthesized gold nanoparticles were functionalised with a capping agent to increase their colloidal stability and to provide an intermediate ligand for protein bioconjugation. For this purpose, 11-mercaptoundecanoic acid (MUA) was used since the thiol group adsorbs strongly on gold substrates and sucessfully disperses the nanoparticles in solution at neutral pH values [26].

An ethanolic solution of MUA at 10 mM was prepared and a suitable volume was added to the gold nanoparticles suspension to attain a molar ratio of 3500. The solution was kept under vigurous stirring at 700 rpm for 15 minutes. The resulting solution was kept in the fridge overnight to ensure a complete layer formation on top of the

nanoparticles. Several centrifugations at 9500 *g* for 10 minutes were needed to remove excess MUA due to the small size of the nanoparticles. The pellets were resuspended in ultrapure water and stored in the fridge, away from sunlight.

2.1.4. Dynamic Light Scattering (DLS) measurements

Dynamic light scattering measurements were taken in order to determine the polydispersity and hydrodynamic diameter of the nanoparticles in colloidal suspensions. The measurements were performed in a SZ-100 Nanopartica series (Horiba, Japan) with a 4 mW (532 nm) He-Ne laser at scattering angles of 90° and 172°. A volume of 800 µl of dilluted sample was transferred to a quartz cell with 1 cm pathlength. Each sample was measured 5 times at 25°C.

2.1.5. AuNPs colloidal stability

In order to test the nanoparticles' stability in colloidal form for their future use in the lateral flow assay, several experiments were performed. First, their stabilty over time was measured by taking several UV-Vis spectra at 1, 2, 5, 7 and 27 days post synthesis. Because blood has a sodium concentration of 135-145 mM [27], several suspensions were prepared with increasing concentratrions of NaCl, from 10 to 250 mM. In order to test the nanoparticles' stability in various pH conditions, several suspensions with a pH between 1.6 and 10.8 were prepared using 0.1 M HCl solution and 0.1 M KOH solution, respectively. The UV-Vis spectrum of each solution was taken and the aggregation index was calculated by dividing the absorbance value at the LSPR and the absorbance at 600 nm.

$$Agg_{index} = \frac{A_{600}}{A_{LSPR}} \tag{2.4}$$

2.2. Development and characterization of bioconjugates with Human Serum Albumin (HSA)

2.2.1. Bicinchoninc acid assay for total protein determination

The total amount of protein was checked for every aliquot used, in order to be able to accurately measure the amount used in experiments. The protein concentration was determined by a bicinchoninic acid assay (BCA) based on a method developed by Smith *et al* [28]. The method is comprised of two stages: *(i)* the reduction of Cu^{2+} to Cu^{+} by a protein in an alkaline environment and *(ii)* a colorimetric detection of the Cu^{+} cation using a reagent containing bicinchoninic acid. The solution changes colour from green to purple based on the amount of protein it contains, which can be measured as a change in absorbance at 562 nm using a UV-Vis spectrophotometer. By using known amounts of protein, a standard curve can be calculated, thus allowing the quantification of the unknown amount of protein in the samples measured.

Bovine serum albumin (BSA) protein standard (≥98%, Sigma-Aldrich, USA) was used for the standard curve determination, in a series of dillutions of known amounts (0 to 30 µg protein). The working reagent was prepared by mixing a volume of 49 ml BCA solution with 1 ml $CuSO_4$. The unknown samples were prepared in dillutions in such a way that the expected amount will fit in the middle part of the curve (1:2 – 1:20 depending on the aliquot and the sample measured).

A volume of 1 ml BCA reagent was added in each Eppendorf tube with the proper amount of BSA protein standard and unknown sample to obtain the desired dillutions. The tubes were vortexed and incubated at 37°C for 30 minutes. [29] The samples were left to cool to room temperature. The absorbance at 562 nm was measured for all solutions very quickly, so as the total time from the first measurement to the last did not exceed 10 minutes. The measurements were plotted, thus determining the standard curve and the unknown concentrations were determined.

2.2.2. Conjugation through physisorption

The AuNPs were conjugated with HSA by preparing several aliquots of 3 nM nanoparticles solutions in 5 mM potassium phosphate buffer (KPB) and letting them incubate overnight at 4°C. The samples were centrifuged at 9500 g for 20 minutes, the supernatant discarded and the pellets resuspended in 20 mM KPB solution. The proper amount of protein for the formation of a full corona on the nanoparticles was assessed through electrophoretic assays.

2.2.3. Agarose Gel Electrophoresis (AGE)

AGE measurements were taken to measure the electrophoretic mobility of the samples in order to assess the proper amount of protein for full corona formation. For all experiments, UltraPure Agarose (Invitrogen, Thermo Fisher Scientific, USA) was used at 0.5% (w/v) in 1:8X Tris-Acetate-EDTA (TAE) buffer at pH 8. The solution was heated under gentle stirring at 80°C until the liquid became translucid. The liquid was poured in a gel tray (mini-sub cell GT, Bio-Rad, Portugal) with a tooth comb and cooled down until solidification, for 30-90 minutes at 4°C. Afterwards, the tray was set in the AGE chamber and immersed in 1:8X TAE buffer.

The samples were centrifuged at 9500 *g* at 4°C for 20 minutes. The supernatant was discarded and the pellet was resupended in 20 µl of 10% glycerine and 20 mM KPB solution. A volume of 20 µl of each sample was placed in the gel. The AGE was performed with a voltage of 80 V for 80 minutes. The analysis was made using ImageJ.

2.3. Development and characterization of bioconjugates with anti - Horseradish Peroxidase (aHRP)

2.3.1. Conjugation through physisorption

The AuNPs were conjugated with aHRP by preparing several aliquots of 2 nM nanoparticles solutions in 5 mM KPB solution and letting them incubate in an orbital shaker at 250 rpm, 25°C for 90 minutes. The samples were centrifuged at 9500 *g,* 4°C for 20 minutes, the supernatant discarded and the pellets resuspended in 20 mM KPB solution. The proper amount of antibody for the formation of a full corona on the nanoparticles was assessed through AGE assays. The conjugates were further incubated with BSA in the same concentration and conditions as the antibodies, in order to block the binding sites unoccupied by the antibodies and stop non-specific binding.

2.3.2. Conjugation through covalent linking

The AuNPs were covalently conjugated with aHRP via carbodiimide activation chemistry, through the use of EDC/SHNS. EDC activates the carboxyl group on the nanoparticles' surface in order to create a crosslinker. This intermediate form is unstable and prone to hydrolysis. By adding SNHS, a stable amine-reactive bond is formed, which will in turn bind to the primary amines on the antibody. [30] EDC at 0.06 nM was added to several aliquots of 2 ml AuNPs at 10 nM, followed by SHNS at 0.13 nM and the samples were left to incubate for 15 minutes. The samples were then centrifuged at 9500 *g,* 4°C for 20 minutes to remove the spent carbomiide. The next step was to add the antibodies and let the samples incubate as previously described for the physisorbed conjugation.

2.3.3. HRP enzymatic activity assay

The binding of the antigens to the bioconjugates is dependant on the proper orientation of the antibodies on the AuNPs' surface. Enzymatic activity assays were employed to determine the successful binding of peroxidase antigens to the bioconjugates, in order to assess the proper conjugation of aHRP antibodies to the AuNPs.

Peroxidase is the catalyst of the oxidoreduction reaction between hydrogen peroxide solution (H_2O_2) and ABTS. The protocol used is based on the Sigma-Aldrich one. [31] The reaction is measured through UV-Vis spectra at 405 nm, for approximately 3 minutes.

A fresh solution of 9.1 mM ABTS in 10 mM KPB was prepared for each assay. A volume of 17 µl of sample and 34 µl of H_2O_2 (0.3% v/v) were added. The solution was quickly mixed by inversion and introduced in the spectrophotometer for the measurement.

The peroxidase activity is calculated with the following equation:

$$Units/mg_{solid} = \frac{\left(\Delta A_{405\,nm}/\min(test) - \Delta A_{405\,nm}/\min(blank)\right) * V_{final} * DF}{\varepsilon * V_{blank/enzyme}} \quad (2.5)$$

DF is the dillution factor, V_{final} is the final volume of the solution, V_{blank} is 17 µl of sample. $\Delta A_{405\,nm}/min$ were calculated from the slope of the curve obtained using the maximum linear rate for both test and blank. The extinction coefficient ε of oxidised ABTS at 405 nm is 36.8 $mM^{-1}cm^{-1}$ [31]

2.4. Lateral Flow Assay fabrication

2.4.1. Lateral flow dispenser

For precise dispensing of the antibodies solutions on the test and control lines, a lateral flow dispenser was designed in Catia V5 (Dassault Systemes, France).

2.4.2. Membrane selection

For the lateral flow assay assembly, a starter kit (Advanced Microdevices, India) was used. The kit contains absorbant pads, nitrocellulose membranes, conjugate pads and sample pads. A Nature protocol was followed for the iterative optimisation of the assay. [19] As such, the first step was to select the right membrane and absorbent pad for the application. The two types of absorbent pad available had different thicknesses, which impacts the volume of sample they can hold, as well as the wicking time. The absorbant pad with the lowest thickness (AP-045, 0.4 mm) was used to slow down the capilar flow of the sample and allow it to react longer with the test and control line. The kit contains three types of nitrocellulose membranes with different pore sizes, protein binding capabilites and wicking times.

Low protein binding	**Pore sizes**			
CNPF	8 µm		10 µm	
High protein binding	**Pore sizes**			
CNPC	12 µm		15 µm	
Highest protein binding	**Wicking times**			
CNPH	70 s	90 s	150 s	200 s

Table 2.1. Types of nitrocellulose membranes from the starter kit

All components were cut manually into 3 x 0.5 cm (absorbent pads) and 6 x 0.5 cm (nitrocellulose membrane) and assembled together. The test and control antibodies were spotted manually by depositing 1 µl of 1 mg/ml aHRP antibodies and 1 µl of 1 mg/ml anti-IgG antibodies (ImmunoPure Mouse IgG, Thermo Fisher Scientific, USA). The membrane was left to dry for 30 minutes at room temperature after which it was incubated with 600 µl of AuNP-aHRP bioconjugates and peroxidase at 0.04 mg/ml.

A blocking step was also tested by incubating the nitrocellulose membrane with skim milk (2%, w/v) for 30 minutes at room temperature, washed 3 times with PBS-Tween (0.01 M PBS, Tween 20 at 0.05% w/v) and dried at 37°C for 30 minutes.

3. Results and discussion

3.1. Gold nanoparticles

3.1.1. Synthesis and characterization

The spherical nanoparticles were synthesised based on a modified version of the Turkevich method [21], as developed by Ojea-Jimenez [22], in which the citrate is added before the chloroauric acid – the order of the reagents being changed. That results in a better size control and a more uniform distribution of shapes and sizes.

Figure 3.1 The synthesis set-up: a round bottom flask on top of a heating plate under reflux

Immediately after synthesis, there was visual confirmation of success, as shown in Figure 3.2, the deep red colour being a good indicator of disperse gold nanoparticles of around 20 nm in size. [32]

Figure 3.2 A fresh solution of citrate capped gold nanoparticles

The nanoparticles were characterised through UV-Vis spectroscopy, where it is possible to identify their LSPR peak at 520 nm. Their stability was measured in time, the spectra remaining at around 520 for at least a month, as shown in Figure 3.3. The intensity at 600 nm is a good indicator of the aggregation status of the solution, in this case showing no increase over time and thus a good colloidal stability of the nanoparticles.

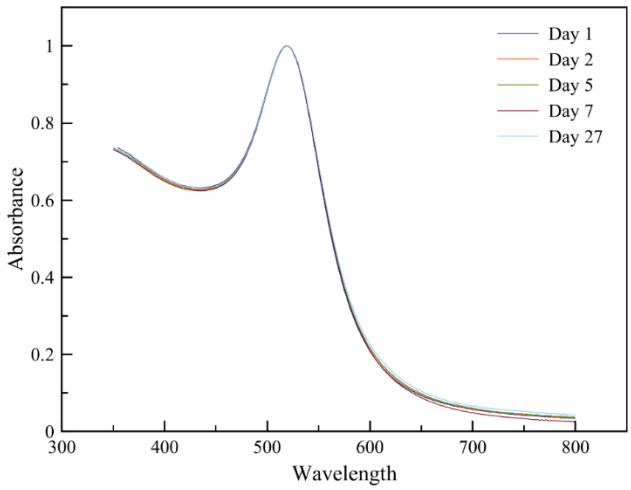

Figure 3.3 UV-Vis spectra of the nanoparticles taken over 27 days, indicating good colloidal stability

The diameter of the nanoparticles was determined by the method devised by Haiss et al. [24], resulting in a 12.2 ± 0.2 nm diameter. The concentration was calculated through the Beer-Lambert law [25], resulting in 16.2 nM.

3.1.2. Modification with 11-MUA

The AuNPs were modified by coating them with 11-MUA to increase their stability, as well as provide a linker for protein binding. The success of the modification was checked through UV-Vis spectra, as well as DLS measurements.

As shown in Figure 3.4, the UV-Vis spectra shows a red shift of 4 nm, the new LSPR peak appearing at 524 nm. There is also a slight increase in the intensity at 600 nm, indicating a small amount of aggregation. The DLS measurements show an increase in the hydrodynamic diameter of the nanoparticles, from an average of 12 nm to 15 nm. The polydispersity index also shows a slight increase, from 0.1 to 0.2, confirming the scarce presence of aggregates indicated by the UV-Vis spectra.

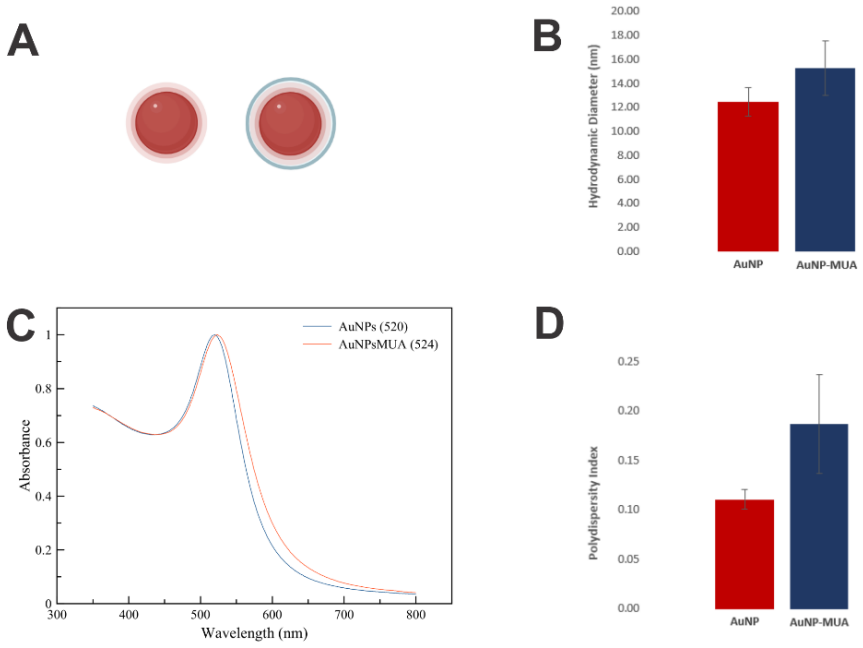

Figure 3.4 A. Schematic drawing of AuNPs and AuNP-MUA; B. Hydrodynamic diameter of AuNPs and AuNP-MUA as shown by DLS measurements; C. UV-Vis spectra of AuNPs and AuNP-MUA; D. Polydispersity index of AuNPs and AuNP-MUA

3.1.3. Colloid stability

In order to make assure the stability of the nanoparticles in various environments, as well as confirm a full coating of mercaptoundecanoic acid, the colloid was tested against different salt and pH levels.

The addition of NaCl to the colloidal solution reduces the surface charge of the nanoparticles, making them unstable and prone to aggregation. [33] By varying the pH of the solutions, the pKa values of the coating agent (citrate or 11-MUA) can be equaled, and thus the surface charge of the nanoparticles changes, causing them to aggregate. [34]

The stability in salt was measured by preparing samples of AuNPs and AuNP-MUA at 2 nM with varying concentrations of NaCl, from 0 to 250 mM. After the addition of the salts, the solutions were measured with UV-Vis spectroscopy. The aggregation index was measured as the ratio between the absorbance at the LSPR and the absorbance at 600 nm.

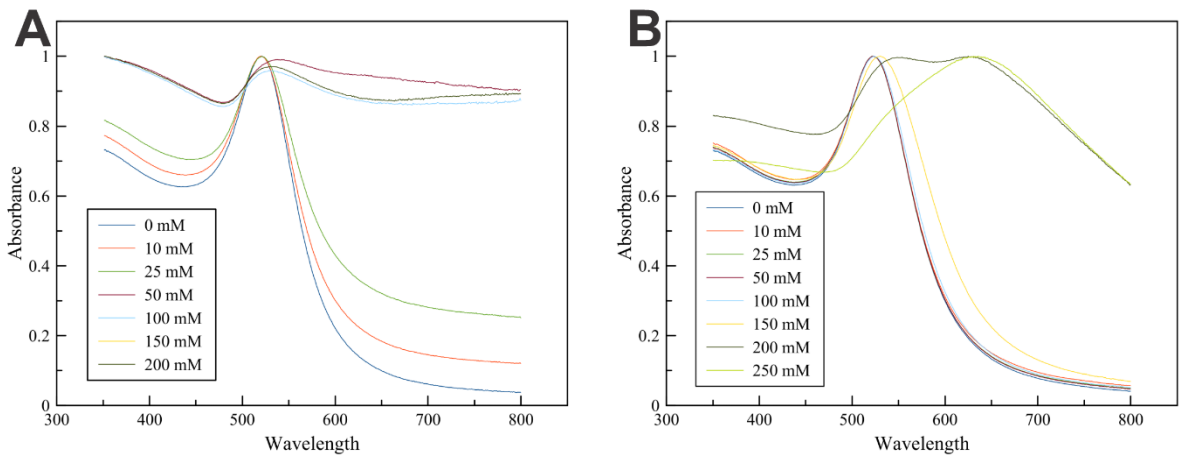

Figure 3.5 A. UV-Vis spectra of AuNPs with different NaCl concentratrions (0-200 mM); B. UV-Vis spectra of AuNP-MUA with different NaCl concentratrions (0-250 mM)

We can observe that the AuNPs samples exhibit a red-shift after 25 mM, with a significant increase in the absorbance at 600 nm indicating aggregation. However, for the coated nanoparticles, the shift appears only at 150 mM, showing high stability up to that concentration of NaCl.

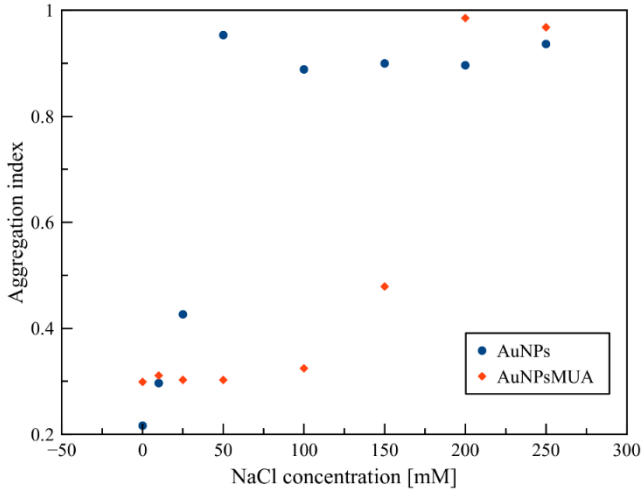

Figure 3.6 Aggregation index calculated through the UV-Vis spectrum against different salt concentrations for AuNPs and AuNP-MUA

We can observe that the aggregation index increases abruptly for the uncoated nanoparticles, but remains stable for the AuNP-MUA solutions up to a concentration of 150 mM. Because the immunotags are to be used with blood samples, which has a concentration of salt of approximately 135-145 mM [35], and the subsequent coating of antibodies will provide additional stability, we can conclude that the nanoparticles will be stable for test use.

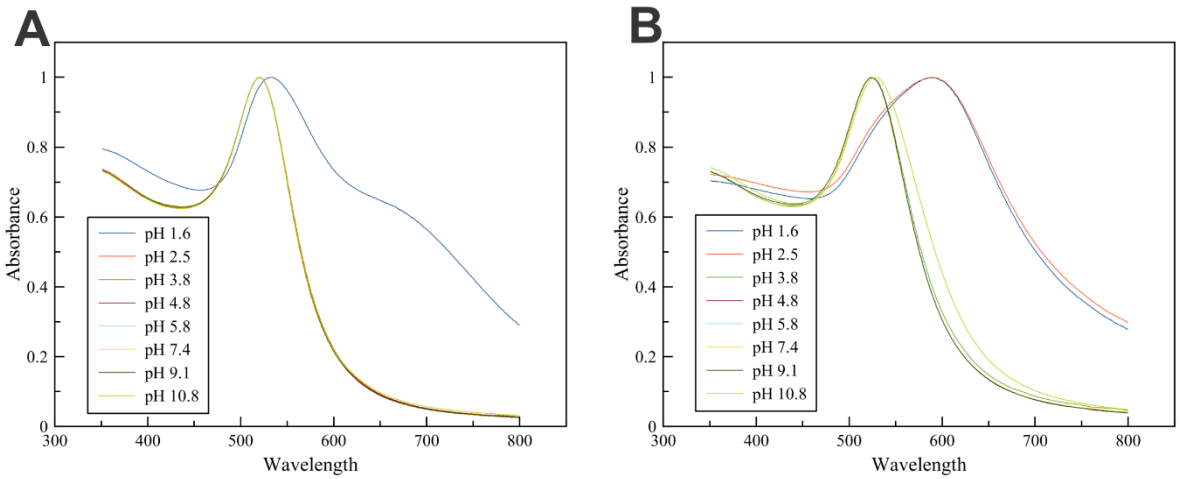

Figure 3.7 UV-Vis spectra of AuNPs in solutions with varying pH (1-10); B. UV-Vis spectra of AuNP-MUA in solutions with varying pH (1-10)

The stability in pH was tested similarly, the gold nanoparticles showing high stability for pH levels up to a very acidic pH of 1.6, while the coated nanoparticles showed a lower stability, remaining unaggregated only up until a pH of 2.5. The difference can be attributed to the pKa point of citrate versus mercaptoundecanoic acid. However, since blood has a normal pH of 7.35-7.45 [36], we can conclude that the nanoparticles will be stable for test use.

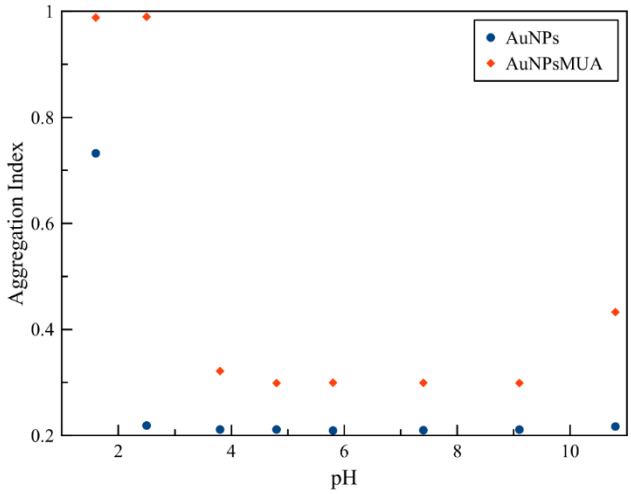

Figure 3.8 Aggregation index calculated through the UV-Vis spectrum against different pH levels for AuNPs and AuNP-MUA

3.2. Bioconjugates with HSA

3.2.1. Bicinchoninic acid assay for total protein determination

A standard protein curve was used to measure the concentration of human serum albumin, horseradish peroxidase, anti-horseradish peroxidase and bovine serum albumin for each new aliquot that was used. A new BCA curve was calculated as explained in section 2.2.1 for each new batch and the total protein concentration was measured by using the equation obtained from the curve.

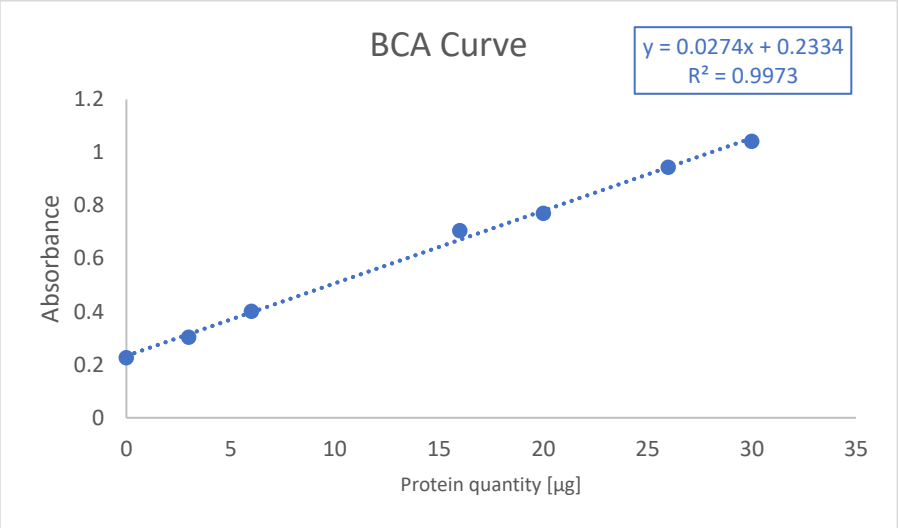

Figure 3.9 BCA curve with protein standard BSA with amounts from 0 to 30 µg

3.2.2. Conjugation through physisorption

In order to optimise the conjugation process, the first step was to assess the sufficient amount of protein that will form a full corona around the nanoparticles. The proteins were incubated overnight with increasing concentrations of human serum albumin. Agarose gel electrophoresis measurements were taken and the electrophoretic mobilities of the conjugates were fitted using a Hill type isotherm.

The migration in each lane was measured using ImageJ, by measuring the distance from the well to the front of the band. The electrophoretic mobility can be calculated by dividing the migration velocity to the strength of the electric field that drives the motion, as shown in the following equation:

$$\Delta\mu = \frac{v}{E} \tag{3.1}$$

The velocity was calculated by dividing the distance measured in ImageJ by the running time of the gel. The electric field was calculated by dividing the voltage to the distance between the electrodes.

The resulting data was plotted with the HSA concentrations and fitted to a Hill isotherm, based on the following equation [37]:

$$\Delta\mu = \frac{\Delta\mu_{max} * x^n}{K_D^n + x^n} \tag{3.2}$$

where $\Delta\mu$ is the difference between the electrophoretic mobility of the data point and the control sample, x is the concentration of protein conjugated with the nanoparticles, K_D is the dissociation constant which correlates the value of the concentration for half $\Delta\mu_{max}$. n is the cooperativity parameter, which defines a positive (>1) or negative (<1) cooperativity describing whether a bound protein favours the binding of another or not.

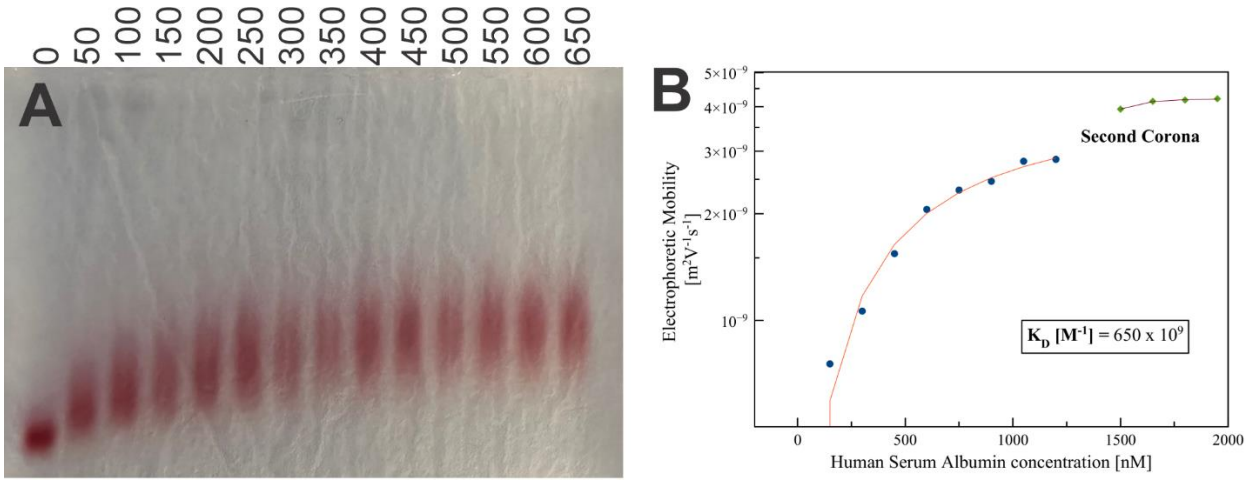

Figure 3.10 A. AGE of AuNP-HSA with different protein to nanoparticle ratios; B. The calculated electrophoretic mobilities fitted with a Hill isotherm

Figure 3.10 presents the electrophoretic mobilities calculated from the AGE and fitted with an isotherm. It can be observed that after a certain amount of protein, the corona is formed, the slope coming to a plateau. After the fitting, it was discovered that after a ratio of protein to nanoparticles of 500, there is a jump in the electrophoretic mobilities, which we have ascribed to the formation of a second protein corona. The fitting resulted in a value for the dissociation constant $K_D = 650\ nM^{-1}$, corresponding to a ratio of 1:325 for the formation of a full protein coating.

3.3. Bioconjugates with aHRP

3.3.1. Conjugation through physisorption

The nanoparticles were incubated with different concentrations of anti-horseradish peroxidase antibodies in order to assess the proper amount of antibodies needed to fully coat them. The experiments were done similarly to those for HSA, the incubation protocol being as described in section 2.3. The agarose gel electrophoresis displayed in Figure 3.11 shows bioconjugates with antibodies – nanoparticle ratios between 0 and 100. The ratios were chosen based on the experiments done before with human serum albumin, considering the size difference between the protein and the antibodies (67 kDa [38] vs 150 kDa [39]).

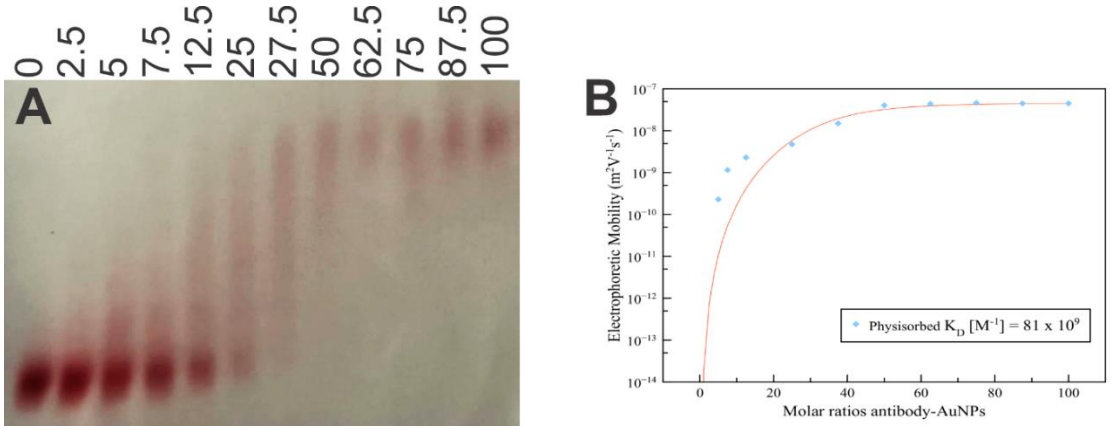

Figure 3.11 A. AGE of physisorbed AuNP-aHRP with increasing ratios of antibodies to nanoparticles; B. Electrophoretic mobilities fitted with a Hill isotherm

It can be observed that for ratios up to 25, the antibodies do not affect the size or negative charge of the nanoparticles since they exhibit a similar electrophoretic mobility to the control sample. We do notice however, that for ratios 5, 7.5 and 12.5 we have two distinct populations, indicating nanoparticles with different amounts of antibodies coating them. The drag that we notice in most bands is due to the inhomogenous coating of the nanoparticles, some being fully coated (at the back of the migration band) and some being coated with a very little amount of antibodies (at the front of the migration band). There was also significant aggregation in the wells, suggesting unstable conjugation.

The fitting with the Hill isotherm suggests a dissociation constant $K_D = 81\, nM^{-1}$, corresponding to a nanoparticles to antibodies ratio of 1:40.

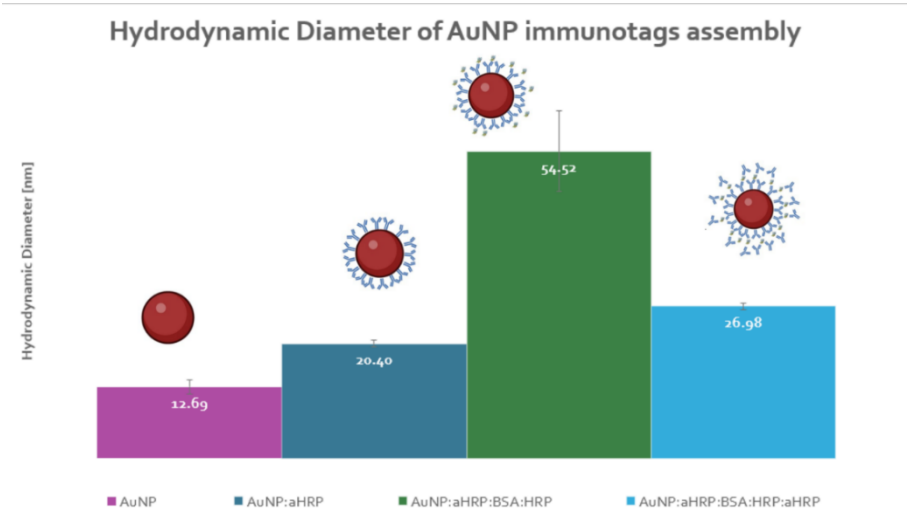

Figure 3.12 DLS measurements of the immunotags displaying their hydrodynamic diameter

The conjugation was further analysed through DLS measurements, using "sandwich" samples which simulate the complexes in a lateral flow assay: control uncoated nanoparticles, antibodies-nanoparticle conjugates, conjugates-sample and conjugates-sample-test antibody. The antibodies to nanoparticles ratio used was 50. In order to avoid non-specific binding, the conjugates were blocked with BSA in the same concentration as the antibodies, as described in section 2.3.1. The expected trend would be an increase in the hydrodynamic diameter, corresponding to the proper binding of the antibodies and protein. We can observe from Figure 3.12 however, that after incubating the conjugates with the target protein and antibodies, the hydrodynamic diameter decreases. That suggests that the second antibodies capture the protein-antibody complex that was bound to the nanoparticles, and due to a weak link between the nanoparticles and the antibody coating, they break free in the solution. This further indicates that antibodies bound through physisorption create unstable bioconjugates that could not be used in lateral flow assays.

To determine the binding of the peroxidase to the antibodies with the correct orientation, an enzymatic activity assay was performed. The samples with antibodies and protein, antibodies – protein – antibodies and antibodies – antibodies were tested with the assay after incubation and washing. The activity was measured as explained in

section 2.3.3, by measuring the absorbance at 405 nm for 3 minutes. As shown in Figure 3.13, the immunotags with HRP and the sandwich sample (aHRP-HRP-aHRP) display a small amount of activity, most likely due to the improper binding of the antibodies, making the binding sites for the protein unavailable. Another possible explanation is that because the physisorption conjugation provides a weak bond, during the washing step many of the antibodies are lost. The sample with aHRP – aHRP displays negative activity due to the lack of protein present, which is as expected.

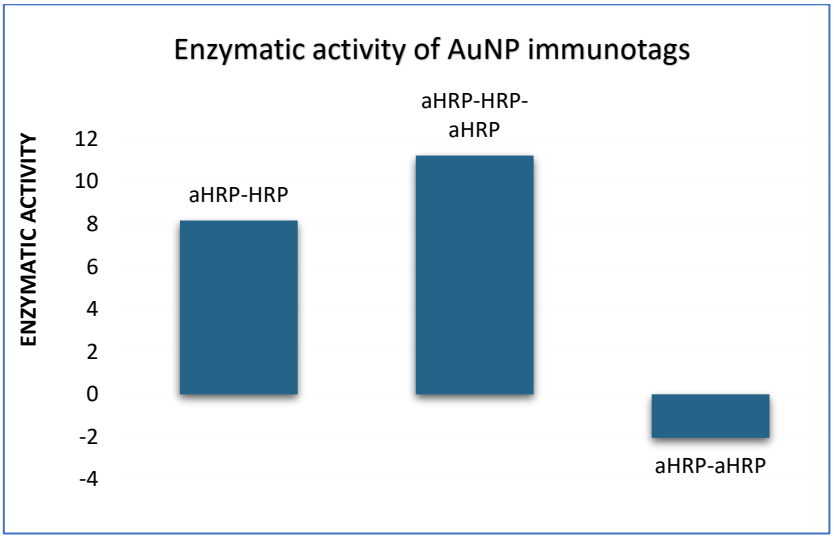

Figure 3.13 Enzymatic activity assay of the immunotags

3.3.2. *Conjugation through covalent linking

**This subchapter is presented with the approval of Nuno Ferreira who has performed the experiments pertaining to exploring bioconjugation through covalent linking.*

In order to increase the stability of the bioconjugates and strengthen the bond between the antibodies and nanoparticles, a covalent conjugation was advanced. The nanoparticles were conjugated with EDC/SNHS, as described in section 2.3.2, which resulted in a covalent bond betweeen the amine group of the antibody and the carboxylic group from the AuNP-MUA. The bond is thus much stronger than through physisorption and the antibodies remain attached to the nanoparticles after washing and incubating with the target protein.

Similarly to the experiments done to assess physisorbed conjugates, several ratios of antibodies to nanoparticles were tested. It can be noticed from the AGE that we have considerable drag in all migration bands, indicating conjugates with varying amounts of antibodies coating them. The electrophoretic mobility of the bioconjugates was assessed by choosing the most intense point in the band based on an intensity profile in ImageJ. The Hill isotherm fit resulted in a dissociation constant $K_D = 35\ nM^{-1}$, which is in line with results found in the literature. [40]

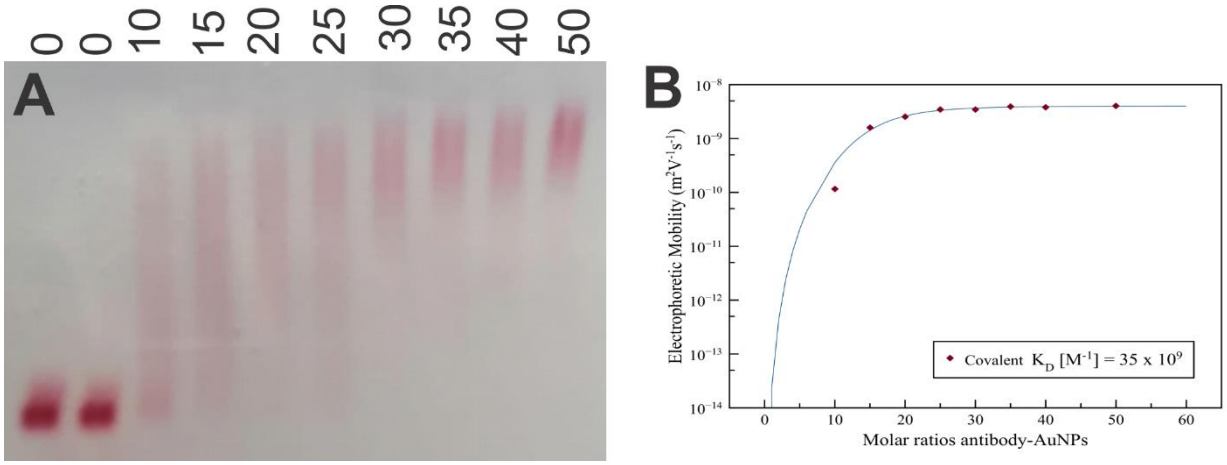

Figure 3.14 A. AGE of covalently linked AuNP-aHRP with increasing ratios of antibodies to nanoparticles; B. Electrophoretic mobilities fitted with a Hill isotherm *(experiments performed by Nuno Ferreira)*

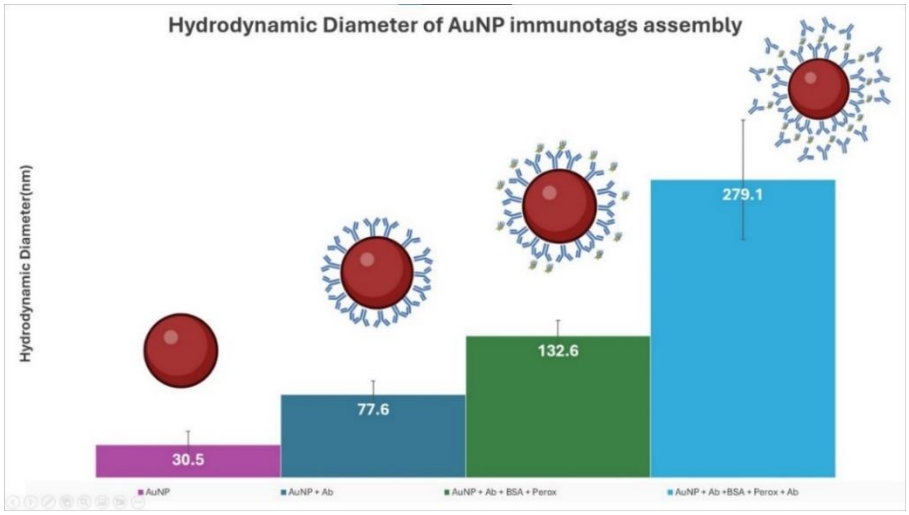

Figure 3.15 DLS measurement of the immunotags displaying increasing hydrodynamic diameter *(experiments performed by Nuno Ferreira)*

DLS measurements were perfomed similarly to those with physisorbed conjugates, for a nanoparticles – antibodies ratio of 1:50. It can be observed in Figure

3.15 that the ascending trend we were expecting is present, indicating that the antibodies are strongly bound to the nanoparticles and the bond is not broken by the addition of the secondary antibodies. This suggests a successful functionalisation and the possible future use in a lateral flow assay.

The enzymatic activity assay was performed for increasing ratios of antibodies to nanoparticles and the ascending trend indicates that the antibodies bind in the proper orientation on the nanoparticles, thus allowing the protein to attach to its specific binding sites.

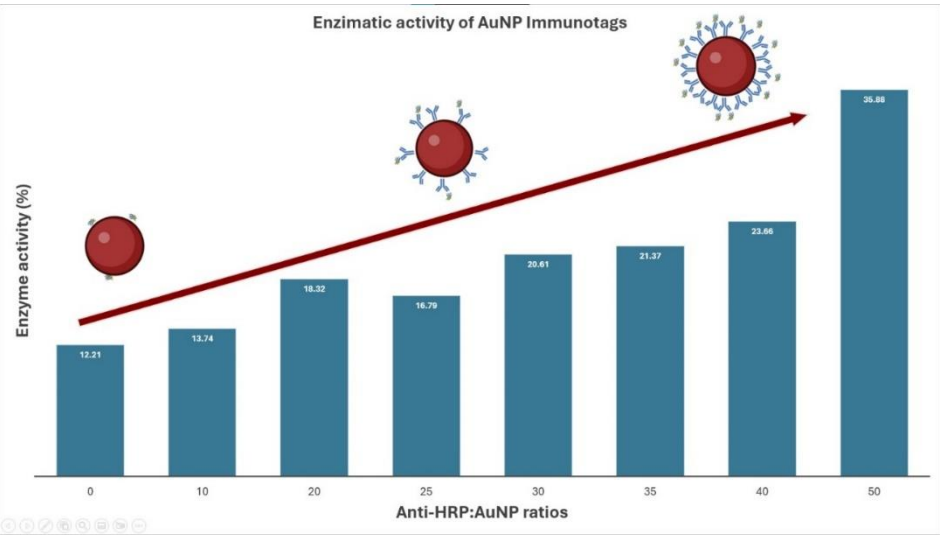

Figure 3.16 Enzymatic activity assay of immunotags with increasing antibodies to nanoparticles ratios *(experiments performed by Nuno Ferreira)*

3.4. Lateral Flow assay fabrication

3.4.1. Lateral Flow Dispenser

In order to achieve reproducible results, the test and control line would need to be drawn automatically to exclude human error. For that purpose, a lateral flow dispenser was designed from scratch in a CAD software, with components that could be 3D printed and largely available mechanical and electronical parts which makes it very cost friendly.

The working principle of the device is based on two syringes that drive the flow of the solutions through tubing up to a dispensing head that moves laterally, allowing the precise “drawing” of the two lines on the nitrocellulose membrane.

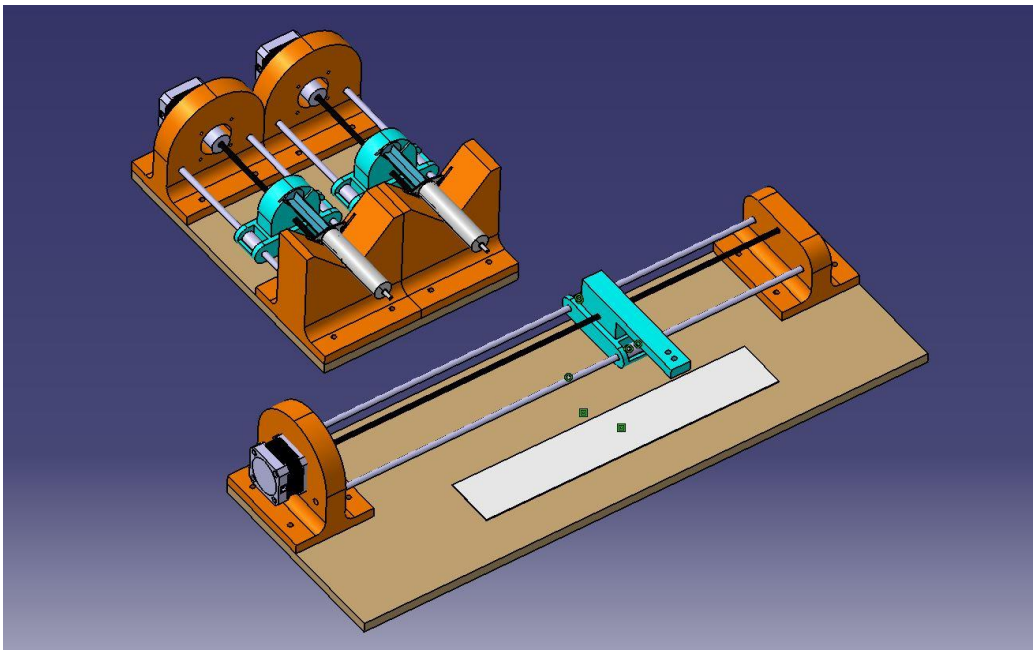

Figure 3.17 Lateral flow dispenser design

Mechanically, the two syringes and the lateral dispenser are all actuated through nut-screw mechanisms. A stepper motor turns a threaded rod at a calculated pace which in turn moves the carriage that holds the equipment. The entire circuit is commanded through a programmable board such as Arduino or Raspberry Pi.

The device has not been built, remaining in the design phase but it remains one of the avenues to be explored in the future in order to improve the quality and reproducibility of the LFAs.

3.4.2. Membrane selection

Of the eight types of nitrocellulose membranes available, two were tested for use in this lateral flow assay application, based on previous work done by Ana Tomás. [41] CNPH-150 and CNPH-200, high protein binding membranes with wicking times of 150 s and 200

s were cut into strips and assembled with absorbent pad AP-045. The test and control antibodies solutions were spotted manually on the membrane and the half-stick tests were left to dry as previously described in section 2.4.2.

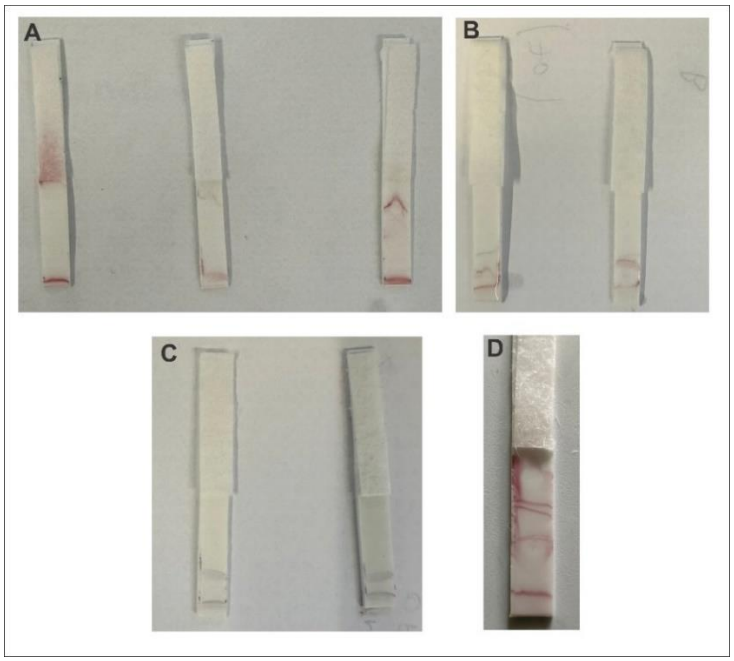

Figure 3.18 Nitrocellulose membranes with different wicking times, different concentrations of immunotags and different running buffers. A. CNPH-150 [AuNP-aHRP] = 2,3,4 nM, KPB; B. CNPH-150 [AuNP-aHRP] = 1, 0.75 nM, KPB; C. CNPH-150 [AuNP-aHRP] = 1, 0.75 nM, PBS; D. CNPH-200, [AuNP-aHRP] = 2 nM, KPB, blocked with skim milk

The membranes were analysed by visual inspection, however the bioconjugates did not flow towards the absorbent pad properly. Figure 3.18 presents several experiments with different variables done in an attempt to find the cause of the poor flow of the immunotags. Several concentrations were tested, from 0.75 nM to 4 nM, although none were found to be satisfacatory, as well as different buffers – KPB and PBS. The bioconjugates in PBS aggregated, which can be noticed visually by the change in colour – from red to blue.

It can be observed that the bioconjugates adhere to the nitrocellulose membrane and remain bound in a line at the bottom. That could be explained by the non-specific binding of the nanoparticles to the nitrocellulose. An additional step of blocking the membrane with skim milk was tested in order to reduce the non-specific interactions. Nevertheless, it did not greatly improve the flow of the sample, as can be seen in Figure 3.8 D.

Conclusions and future perspectives

This research aimed to develop an innovative diagnostic method for traumatic brain injuries (TBIs). A lateral flow assay (LFA) was selected as the testing platform, using glial fibrillary acidic protein (GFAP) as a promising biomarker. The development process encompassed the creation of immunotags—bioconjugates of gold nanoparticles (AuNPs) and antibodies—followed by testing in sandwich assays which simulate test line antibodies, and ultimately evaluation in an LFA format.

Gold nanoparticles of 12 nm diameter were synthesized and modified with mercaptoundecanoic acid (11-MUA) to enhance stability and provide better protein binding capabilities. Colloidal stability was confirmed under various pH and salt conditions, demonstrating the bioconjugates' robustness in a blood-mimicking environment, which will be the LFA sample matrix. Stability over time was also assessed, the nanoparticles remaining stable for at least one month.

To determine the optimal antibody amount for a full protein corona, AuNPs-MUA were incubated with increasing ratios of anti-horseradish peroxidase antibodies. Agarose gel electrophoresis was used to evaluate electrophoretic mobility, and a Hill-type isotherm analysis identified a nanoparticle-to-antibody ratio of 1:50 as optimal. Both physisorption and covalent binding strategies were explored, with EDC/SNHS-mediated covalent linking proving superior. This method not only ensured the stability of the conjugates, the antibodies remaining attached post-centrifugation, but also showed enhanced enzymatic activity, indicating that the antibodies were linked correctly and were able to collect the target protein. Thus, the ideal bioconjugates were established as covalently linked AuNPs-antibodies in a ratio of 1:50.

Several nitrocellulose membranes were tested for LFA compatibility, considering different wicking times, running buffers, and the necessity of a blocking step. The CNPH-200 nitrocellulose membrane, combined with a skim milk blocking step and a 2 nM bioconjugates concentration in KPB, was identified as the best configuration, although issues with proper flow through the membrane persisted, indicating the need for further

optimization. Additionally, a device for accurately dispensing the test and control lines was designed.

The next phase of this research will focus on conjugating the synthesized gold nanoparticles with anti-GFAP antibodies. This step is crucial for creating a diagnostic tool specific to GFAP, a key biomarker for TBIs. The conjugation process will be optimized to ensure maximum binding efficiency and stability, employing the covalent linking method previously determined to be most effective.

Furthermore, extensive testing with lateral flow assays will be conducted to fine-tune the conditions under which the assay operates. This includes optimizing the incubation times, antibody concentrations, and the running buffer composition. Special attention will be given to improving the flow through the nitrocellulose membrane, addressing the current issue of incomplete sample migration.

Building a robust and reliable lateral flow dispensing device is another critical future step. This device will be engineered to accurately dispense test and control lines, ensuring consistent and reproducible results. The device's design will be refined based on the outcomes of initial trials, aiming for ease of use and scalability for potential mass production.

Additionally, the assay's performance will be validated using clinical samples to confirm its efficacy and reliability in real-world conditions. This validation process will involve collaboration with healthcare institutions to obtain and test blood samples from patients with confirmed TBIs.

In conclusion, this research demonstrates significant potential for developing a rapid, reliable, point-of-care test for traumatic brain injuries. Such a test could substantially reduce the burden on healthcare systems by providing a cost-effective and efficient diagnostic tool. The groundwork laid by this study offers a promising foundation for further development, with the ultimate goal of creating a widely accessible diagnostic assay that can deliver immediate results in clinical settings. The successful implementation of this LFA-based test could revolutionize TBI diagnosis, leading to timely and appropriate medical interventions, ultimately improving patient outcomes and streamlining healthcare delivery.

References

[1] M. C. Dewan *et al.*, "Estimating the global incidence of traumatic brain injury," *J Neurosurg*, vol. 130, no. 4, 2019, doi: 10.3171/2017.10.JNS17352.

[2] A. P. Di Battista *et al.*, "Blood biomarkers in moderate-to-severe traumatic brain injury: Potential utility of a multi-marker approach in characterizing outcome," *Front Neurol*, vol. 6, no. MAY, 2015, doi: 10.3389/fneur.2015.00110.

[3] T. M. Luoto, R. Raj, J. P. Posti, A. J. Gardner, W. J. Panenka, and G. L. Iverson, "A systematic review of the usefulness of glial fibrillary acidic protein for predicting acute intracranial lesions following head trauma," *Frontiers in Neurology*, vol. 8, no. DEC. 2017. doi: 10.3389/fneur.2017.00652.

[4] S. Natarajan and J. Joseph, "A novel time-resolved fluorescent lateral flow immunoassay for quantitative detection of the trauma brain injury biomarker-glial fibrillary acidic protein," *Sensors and Diagnostics*, vol. 1, no. 1, 2022, doi: 10.1039/d1sd00021g.

[5] L. Papa *et al.*, "Evaluating glial and neuronal blood biomarkers GFAP and UCH-L1 as gradients of brain injury in concussive, subconcussive and non-concussive trauma: A prospective cohort study," *BMJ Paediatr Open*, vol. 3, no. 1, 2019, doi: 10.1136/bmjpo-2019-000473.

[6] M. Honda *et al.*, "Serum glial fibrillary acidic protein is a highly specific biomarker for traumatic brain injury in humans compared with S-100B and neuron-specific enolase," *Journal of Trauma - Injury, Infection and Critical Care*, vol. 69, no. 1, 2010, doi: 10.1097/TA.0b013e3181bbd485.

[7] Z. Yang and K. K. W. Wang, "Glial fibrillary acidic protein: From intermediate filament assembly and gliosis to neurobiomarker," *Trends in Neurosciences*, vol. 38, no. 6. 2015. doi: 10.1016/j.tins.2015.04.003.

[8] A. M. Rubiano, N. Carney, R. Chesnut, and J. C. Puyana, “Global neurotrauma research challenges and opportunities,” *Nature*, vol. 527, no. 7578. 2015. doi: 10.1038/nature16035.

[9] J. Ghajar, “Traumatic brain injury,” in *Lancet*, 2000. doi: 10.1016/S0140-6736(00)02689-1.

[10] H. Wolf, S. Frantal, G. Pajenda, J. Leitgeb, K. Sarahrudi, and S. Hajdu, “Analysis of s100 calcium binding protein b serum levels in different types of traumatic intracranial lesions,” *J Neurotrauma*, vol. 32, no. 1, 2015, doi: 10.1089/neu.2013.3202.

[11] L. C. B. Ferreira *et al.*, “Increased levels of interleukin-6, -8 and -10 are associated with fatal outcome following severe traumatic brain injury,” *Brain Inj*, vol. 28, no. 10, 2014, doi: 10.3109/02699052.2014.916818.

[12] M. Honda *et al.*, “Serum glial fibrillary acidic protein is a highly specific biomarker for traumatic brain injury in humans compared with S-100B and neuron-specific enolase,” *Journal of Trauma - Injury, Infection and Critical Care*, vol. 69, no. 1, pp. 104–109, Jul. 2010, doi: 10.1097/TA.0b013e3181bbd485.

[13] R. D. Welch *et al.*, “Modeling the Kinetics of Serum Glial Fibrillary Acidic Protein, Ubiquitin Carboxyl-Terminal Hydrolase-L1, and S100B Concentrations in Patients with Traumatic Brain Injury,” *J Neurotrauma*, vol. 34, no. 11, 2017, doi: 10.1089/neu.2016.4772.

[14] L. F. Eng, R. S. Ghirnikar, and Y. L. Lee, “Glial Fibrillary Acidic Protein: GFAP-Thirty-One Years (1969-2000),” *Neurochem Res*, vol. 25, no. 9–10, 2000, doi: 10.1023/a:1007677003387.

[15] D. O. Okonkwo *et al.*, “GFAP-BDP as an acute diagnostic marker in traumatic brain injury: Results from the prospective transforming research and clinical knowledge in traumatic brain injury study,” *J Neurotrauma*, vol. 30, no. 17, 2013, doi: 10.1089/neu.2013.2883.

[16] M. Creech, L. Carvalho, H. McCoy, J. Jacobs, and H. E. Hinson, “Mass Spectrometry-Based Approaches for Clinical Biomarker Discovery in Traumatic Brain Injury,” *Current Treatment Options in Neurology*, vol. 24, no. 12. 2022. doi: 10.1007/s11940-022-00742-3.

[17] A. Petzold, G. Keir, A. J. E. Green, G. Giovannoni, and E. J. Thompson, “An ELISA for glial fibrillary acidic protein,” *J Immunol Methods*, vol. 287, no. 1–2, 2004, doi: 10.1016/j.jim.2004.01.015.

[18] E. B. Bahadır and M. K. Sezgintürk, “Lateral flow assays: Principles, designs and labels,” *TrAC - Trends in Analytical Chemistry*, vol. 82. 2016. doi: 10.1016/j.trac.2016.06.006.

[19] C. Parolo *et al.*, “Tutorial: design and fabrication of nanoparticle-based lateral-flow immunoassays,” *Nature Protocols*, vol. 15, no. 12. Nature Research, pp. 3788–3816, Dec. 01, 2020. doi: 10.1038/s41596-020-0357-x.

[20] D. Quesada-González and A. Merkoçi, “Nanoparticle-based lateral flow biosensors,” *Biosensors and Bioelectronics*, vol. 73. 2015. doi: 10.1016/j.bios.2015.05.050.

[21] J. Turkevich, “Colloidal gold. Part II,” *Gold Bull*, vol. 18, no. 4, 1985, doi: 10.1007/bf03214694.

[22] I. Ojea-Jiménez, N. G. Bastús, and V. Puntes, “Influence of the sequence of the reagents addition in the citrate-mediated synthesis of gold nanoparticles,” *Journal of Physical Chemistry C*, vol. 115, no. 32, 2011, doi: 10.1021/jp2017242.

[23] W. Lin, R. W. Zhang, S. S. Jang, C. P. Wong, and J. Il Hong, “Organic aqua regia-Powerful liquids for dissolving noble metals,” *Angewandte Chemie - International Edition*, vol. 49, no. 43, 2010, doi: 10.1002/anie.201001244.

[24] W. Haiss, N. T. K. Thanh, J. Aveyard, and D. G. Fernig, “Determination of size and concentration of gold nanoparticles from UV-Vis spectra,” *Anal Chem*, vol. 79, no. 11, 2007, doi: 10.1021/ac0702084.

[25] D. F. Swinehart, “The Beer-Lambert law,” *Journal of Chemical Education*, vol. 39, no. 7. 1962. doi: 10.1021/ed039p333.

[26] S. M. Ansar, S. Chakraborty, and C. L. Kitchens, “pH-responsive mercaptoundecanoic acid functionalized gold nanoparticles and applications in catalysis,” *Nanomaterials*, vol. 8, no. 5, 2018, doi: 10.3390/nano8050339.

[27] P. Strazzullo and C. Leclercq, "Sodium," *Advances in Nutrition*, vol. 5, no. 2, 2014, doi: 10.3945/an.113.005215.

[28] P. K. Smith *et al.*, "Measurement of protein using bicinchoninic acid," *Anal Biochem*, vol. 150, no. 1, 1985, doi: 10.1016/0003-2697(85)90442-7.

[29] "Preparation of the BCA working reagent (WR) Microplate procedure (sample to WR ratio = 1:8).," Https://Assets.Thermofisher.Com/TFS-Assets/LSG/Manuals/MAN0011430_Pierce_BCA_Protein_Asy_UG.Pdf.

[30] "Covalent Conjugation of Antibody to Gold Nanoparticles for Lateral Flow Assays," https://www.fortislife.com/lateral-flow-covalent-conjugation.

[31] "Enzymatic Assay of Peroxidase (EC 1.11.1.7) 2,2'-Azino-bis(3-Ethylbenzthiazoline-6-Sulfonic Acid) as a Substrate," https://www.sigmaaldrich.com/PT/en/technical-documents/protocol/protein-biology/enzyme-activity-assays/enzymatic-assay-of-peroxidase-abts-as-substrate.

[32] S. Alex and A. Tiwari, "Functionalized gold nanoparticles: Synthesis, properties and applications-A review," *J Nanosci Nanotechnol*, vol. 15, no. 3, 2015, doi: 10.1166/jnn.2015.9718.

[33] N. Bizmark and M. A. Ioannidis, "Effects of Ionic Strength on the Colloidal Stability and Interfacial Assembly of Hydrophobic Ethyl Cellulose Nanoparticles," *Langmuir*, vol. 31, no. 34, 2015, doi: 10.1021/acs.langmuir.5b01857.

[34] K. A. Huynh and K. L. Chen, "Aggregation kinetics of citrate and polyvinylpyrrolidone coated silver nanoparticles in monovalent and divalent electrolyte solutions," *Environ Sci Technol*, vol. 45, no. 13, 2011, doi: 10.1021/es200157h.

[35] J. Guillaumin and S. P. DiBartola, "Disorders of Sodium and Water Homeostasis," *Veterinary Clinics of North America - Small Animal Practice*, vol. 47, no. 2. 2017. doi: 10.1016/j.cvsm.2016.10.015.

[36] "Blood pH," *Clinical Veterinary Advisor*, pp. 913–914, 2012, doi: 10.1016/B978-1-4160-9979-6.00368-8.

[37] Ana Sofia Barradas Dalot, “Plasmonic nanostars for sensitive SERS-based immunodetection,” Master Thesis, NOVA University Lisbon, Lisbon, 2022.

[38] V. Mishra and R. J. Heath, “Structural and biochemical features of human serum albumin essential for eukaryotic cell culture,” *International Journal of Molecular Sciences*, vol. 22, no. 16. 2021. doi: 10.3390/ijms22168411.

[39] J. C. a Jr, N. York, and G. Science, “The structure of a typical antibody molecule,” *Immunobiology*, no. 14102, 2001.

[40] M. Cui, R. Liu, Z. Deng, G. Ge, Y. Liu, and L. Xie, “Quantitative study of protein coronas on gold nanoparticles with different surface modifications,” *Nano Res*, vol. 7, no. 3, 2014, doi: 10.1007/s12274-013-0400-0.

[41] A. L. Tomás *et al.*, “Development of a Gold Nanoparticle-Based Lateral-Flow Immunoassay for Pneumocystis Pneumonia Serological Diagnosis at Point-of-Care,” *Front Microbiol*, vol. 10, 2019, doi: 10.3389/fmicb.2019.02917.

DECLARAȚIE PE PROPRIE RĂSPUNDERE

Subsemnatul, Biro Oana Maria, declar că Lucrarea de licență/diplomă/disertație pe care o voi prezenta în cadrul examenului de finalizare a studiilor la Facultatea de Fizică, din cadrul Universității Babeș-Bolyai, în sesiunea iulie 2024 , sub îndrumarea Prof. Dr. Nicolae Leopold, reprezintă o operă personală. Menționez că nu am plagiat o altă lucrare publicată, prezentată public sau un fișier postat pe Internet. Pentru realizarea lucrării am folosit exclusiv bibliografia prezentată și nu am ascuns nici o altă sursă bibliografică sau fișier electronic pe care să le fi folosit la redactarea lucrării.

Prezenta declarație este parte a lucrării și se anexează la aceasta.

21.06.2024

Oana-Maria Biro,